DOI: 10.1002/adma.200701101

A Semi-transparent Plastic Solar Cell Fabricated by a Lamination Process**

By *Jinsong Huang*,* *Gang Li*, and *Yang Yang**

Polymer solar cells have attracted broad research interest because of their advantageous solution processing capability and formation of low-cost, flexible, and large area electronic devices.[1–7] However, the efficiency of polymer solar cells is still low compared to that of inorganic solar cells. Therefore, it is a challenge to find a polymer that has all the required properties for high efficiency devices, such as strong and broad absorption, high carrier mobility, and appropriate energy levels. One possible solution to avoid the strict material requirements is to stack two or more devices with different spectral responses, which enables more efficient utilization of solar energy. Such a solution would require a semitransparent solar-cell device with high efficiency in its absorption wavelength range, while high transparency would be required in the complementary wavelength range. Semitransparent solar cells are also interesting for other appealing applications, such as energy-generating color window glasses.

It is desirable that such solar cell devices can be fabricated using a low-cost strategy, such as the roll-to-roll fabrication process. One critical issue in this fabrication process is how to form the active-layer/cathode mechanic and electronic contacts. The lamination process is one very promising technique to fulfill this requirement owing to its simplicity and low cost. It has been reported to produce two-layer heterojunction solar cells;[1] however, the method is not applicable to bulk heterojunction solar cells, nor compatible with roll-to-roll fabrication process. In this Communication, an electronic glue-based lamination process combined with interface modification is presented as a one-step process for semitransparent polymer solar-cell fabrication. The finished device is metal-free, semitransparent, flexible, self-encapsulated, and highly efficient (with a maximum external quantum efficiency of 70 % and power efficiency of 3 % under AM 1.5 global 1 sun solar illumination conditions with spectral mismatch correction[8]). This approach represents a critical step towards the ultimate goal of low-cost polymer solar cells.

The device fabrication process is illustrated in Figure 1, and can be described by the following steps. In Step I, two transparent substrates coated with a transparent conductor such as indium tin oxide (ITO), fluorine-doped tin oxide (FTO), or a high conductivity polymer, etc., are selected. In Step II, one substrate is coated with a very thin buffer layer (Cs_2CO_3[9,10]) to act as the low-work-function cathode, followed by coating of the active polymer layer. Step III involves the coating of conductive polymer glue to the other transparent substrate. We used modified conducting polymer poly(ethylenedioxythiophene):poly(styrenesulfonate) (PEDOT:PSS) as the electronic glue, which was spin-coated to form the adhesive anode. Step IV is the lamination process: after drying both the substrates, they are laminated together by exerting force so that the two substrates are tightly glued together. During this lamination, a plastic rod with proper hardness rolls the plastic substrate to remove air bubbles. Both substrates are heated to a temperature of 105–120 °C during the lamination process, and the finished devices are then kept on the hotplate for 5–10 min for the final heat treatment.[7] The PEDOT:PSS was purposely modified to become adhesive, so that the two separate films formed good contact at the interface, both electronically and mechanically.[11] In this work, this adhesive and conductive PEDOT:PSS layer was obtained by doping D-sorbitol or volemitol into PEDOT:PSS, as has been successfully demonstrated in polymer light emitting diodes.[11] However, the efficiency of such a device is too low for application. The polymer blend used in this work is regioregular poly(3-hexylthiophene):[6,6]-phenyl-C_{61}-butyric acid methyl ester (RR-P3HT:PCBM) in 1:1 w/w ratio. The 200 nm thick polymer blend film was deposited by the slow-growth method (or solvent annealing) to enhance device efficiency.[7,12,13] Either glass or plastic can be used as the transparent substrate. Figure 1b shows a picture of an all-plastic solar cell. The device area is ca. 40 mm^2. With both cathode and anode being transparent, a semitransparent polymer solar cell is formed. The transparency (T%) of the device is shown in Figure 1c, together with the solar illumination spectrum. A transparency of around 70 % was obtained in the wavelength range where polymer/PCBM has no absorption, which makes this device suitable for application in stacking devices[14] to make full use of the solar spectrum.

This device fabrication method has many advantages over the regular procedure. First of all, no thermal evaporation process is involved in the process, and each layer is coated by a low-cost and easy solution process. Second, in contrast to the reactive metal cathode in regular devices, the cathode in

[*] Prof. Y. Yang, Dr. J. Huang,[+] Dr. G. Li
Department of Materials Science and Engineering
University of California Los Angeles
Los Angeles, CA 90095 (USA)
E-mail: yangy@ucla.edu; jshuang@agiltron.com
[+] Present address: Agiltron Inc., 15 Cabot Rd., Woburn, MA 01801, USA.

[**] This work is financially supported by Solarmer Energy, Inc., and the Air Force Office of Scientific Research.

ADVANCED MATERIALS

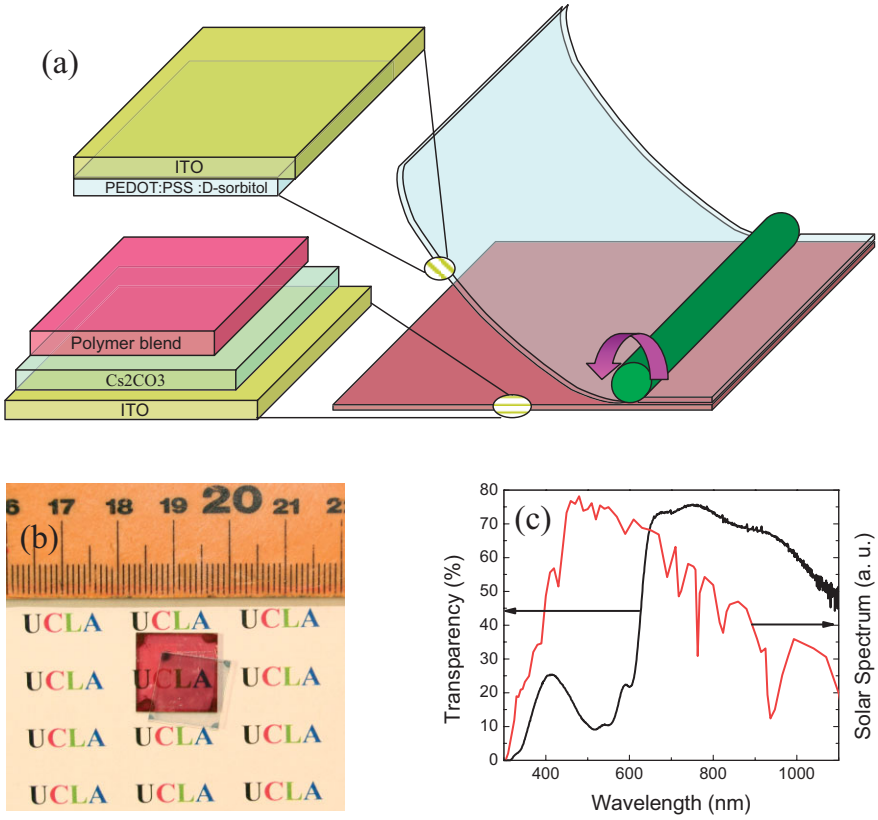

Figure 1. a) Scheme for the device fabrication, b) picture of one device, and c) transparency spectrum of the device and the solar spectrum.

this device is very stable in the air. Third, these devices are self-encapsulated if proper substrates are used. Fourth, this method is potentially easy to be applied for large-area device fabrication through a roll-to roll process. Therefore, all-plastic devices can be realized by using plastic materials for both the substrates.

The devices show high-quality mechanical and electrical contact between the laminated components. For a device area of ca. 40mm^2, the rectification ratio is two to three orders in magnitude at ±2 V, demonstrating good diode behavior. The series resistance of 12±3 Ω·cm^2 is derived from the slope of dark current at a high driving voltage of 2 V, which is several times higher than that of regular device. One possible origin of this higher series resistance is the high resistance of the indium tin oxide (ITO) on plastic substrate used in this work (150 Ω/□ compared to ca. 15 Ω/□ for glass substrate). Despite the high sheet resistance, our laminated device has surprisingly high performance. Photocurrents were measured with light shining from either side of the device, as well as with a piece of white paper placed behind the device. Figure 2a shows the photocurrent density of the device under AM 1.5 simulated illumination of 100 mW cm^{-2} (spectral mismatch corrected). The active area is defined by a photo mask of 4 mm^2. Short circuit current densities (J_{sc}) of 11 mA cm^{-2} from the ITO/PEDOT:PSS side, and 10 mA cm^{-2} from the ITO/Cs_2CO_3 side are obtained. The J_{SC} valeus are actually a littler higher than those obtained from regular devices.[7] Figure 2b shows the external quantum efficiency (EQE) of the device photo-excited from the PEDOT:PSS side with white paper on the back. The purpose of placing a piece of white paper behind the device is to reflect the unused light back to the device for secondary absorption. The maximum EQE obtained is 67 % at 514 nm for the transparent device, which further increases to close to 70 % with a piece of white paper behind the device. One possible reason for the higher EQE than that of regular device is that the high-conductivity PEDOT:PSS anode penetrates into the polymer layer and forms a high-surface-area-structure during the lamination process. Another important contribution for the enhanced EQE might come from during and after lamination. Under this scenario, the hole collection, which is a crucial process in P3HT:PCBM-based devices for high efficiency, will be further enhanced by the increased interface area in this interpenetrating structure. A relatively good fill factor of 55 % indicates that the contact between the polymer blend and PEDOT:PSS layer is actually ohmic. The open-circuit voltage (V_{OC}) of the device is 0.48 V, which is lower than that of regular device (0.6 V), possibly from the reduced work function of PEDOT:PSS by D-sorbital doping,[15] the high resistance of plastic ITO, and/or extra dark current in the unilluminated area. The obtained preliminary power efficiency reaches 3 % under AM 1.5 with spectral mismatch correction. Higher solar cell performance is feasible upon further optimization of parameters, such as the ITO conductivity, the PEDOT:PSS conductivity and the work functions.

The light-intensity-dependent characteristics of the all-solution-processed devices have been studied. Figure 2 c shows the V_{OC}, fill factor (*FF*), responsivity (J_{SC}/I_{light}, where I_{light} is the incident light power density; 100 mW cm^{-2}) and efficiency under incident light power intensity ranging from 0.01–20 suns. Similar to regular devices, the V_{OC} keeps increasing in the full range. With the increased light intensity, *FF* first increases, reaches its maximum of 62 % at half sun, and then begins to decrease at higher light intensity, which should result from the higher series resistance of plastic ITO.[16] Responsivity of the devices remains almost unchanged up to 5 suns, and then begins to decrease after that. The maximum power efficiency of 3.2 % is obtained under 1.5 suns light intensity.

In our device, a Cs_2CO_3 nanolayer plays the crucial role of replacing the low work-function reactive metal cathode, which

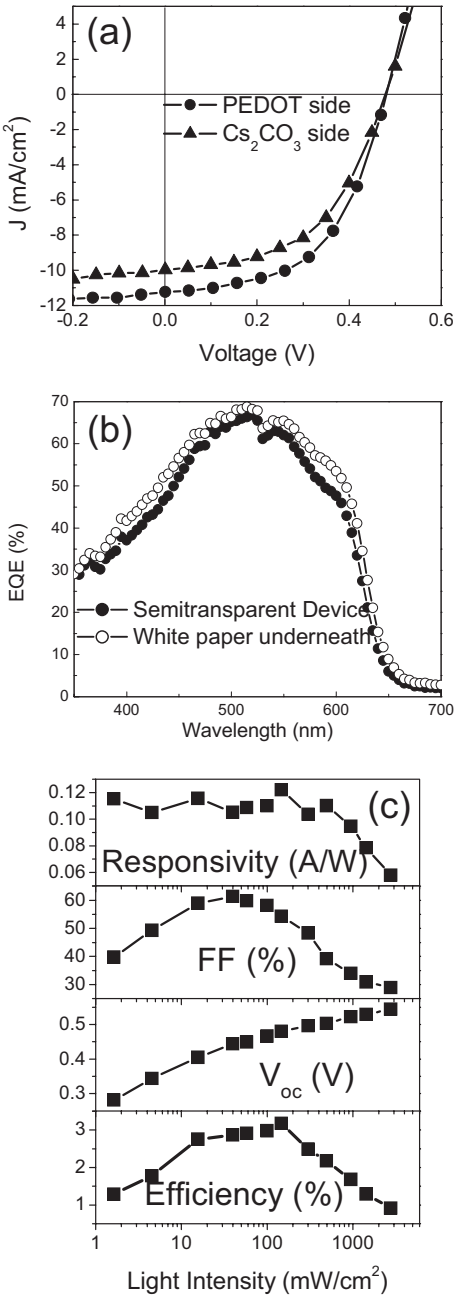

Figure 2. a) Photocurrents under AM 1.5 simulated illumination from front and back side, b) EQE of device with and without a piece of white paper underneath, and c) responsivity, V_{oc}, fill factor (FF), and efficiency of the device under white light intensity from 1–2000 mW cm^{-2}.

makes the all-solution processing possible. Besides Cs_2CO_3, a number of other salts were also evaluated for this layer, including alkali carbonates from Li_2CO_3 to Cs_2CO_3, and cesium-containing salts such as CsF, cesium acetylacetonate [Cs(acac)]. The salts were dissolved in water or polar organic solvent such as 2-ethoxyethanol to form dilute (0.2 wt %) solutions for spin-coating. In order to exclude the effect of high resistance of plastic on device performance, an inverted-structure solar cell[17] was adopted for this evaluation. The inverted polymer solar cells have the structure of ITO/buffer layer/polymer:PCBM/V_2O_5 (10 nm)/Al, where V_2O_5 acts as the anode side and the buffer layer as the cathode. The characteristic parameters of these solar cells with different buffer layers are summarized in Table 1. It is easy to deduce from the table that a thin layer of each of these materials can reduce the work function of ITO or FTO, but to different extents. Two

Table 1. V_{oc}, J_{sc}, and R_s of inverted solar cells using different buffer layer;

	Cs(acac)	CsF	Cs_2CO_3	K_2CO_3	Na_2CO_3	Li_2CO_3	ITO
V_{oc} [V]	0.55	0.54	0.56	0.56	0.50	0.26	0.20
J_{sc} [mA cm^{-2}]	9.64	8.34	9.70	9.62	8.91	8.57	7.01
R_s [O·cm^2]	3.56	4.19	3.50	3.78	8.60	20.3	18.2

distinct behaviors are clearly observed: firstly, for devices with buffer layer from Cs_2CO_3 to Li_2CO_3, the V_{OC} drops, the I_{SC} increases, and the series resistance reduces monotonously; secondly, for the devices with Cs-containing salt buffer layer with different anions [Cs_2CO_3, CsF, and Cs(acac)], all these characteristics are almost the same within the experimental error.

The principle to obtain low work function surface should be completely different from the case of Cs_2CO_3 in PLED devices, where the reaction of Cs_2CO_3 with subsequent deposited Al forms the low-work-function product Cs-O-Al.[18] In order to find out the detailed mechanism of the buffer layers, we conducted X-ray photoemission spectroscopy (XPS)/ultraviolet photoemission spectroscopy (UPS) analysis on the ITO/buffer layer interfaces. The preparations of the samples duplicates real device fabrication steps, i.e., the salts are spin-coated from the dilute aqueous solutions. The thickness of these layers were measured by the decay of X-ray signal intensity of indium according to

$$I = I_0 e^{-L/L_0} \quad (1)$$

where I_0 and I are the indium signal before and after spin-coating of the buffer layer, respectively, L_0 is the free electron path length at a specific energy, and L is the thickness of the buffer layer. The thickness of the spin-coated salts is estimated to be about 0.6–3 nm depending on solution concentration and spin speed. It is clear that there are only a few monolayers of salt molecules on the ITO surface. Figure 3a shows the secondary electron edge of ITO covered by these buffer layers, which provide information about the work function modification of ITO. The work function variation follows one clear trend: the work function of ITO substrates reduces with buffer layers from Li-containing to Cs-containing salts, and buffer layers containing the same metal ion give almost the same work function, which agrees well with the inverted solar cell performance. It is easy to infer that the work function is related only to the metal ions in the salt. Because there is a large change in the work function with the addition of only a few monolayers of molecules, it is believed that strong dipole

ADVANCED MATERIALS

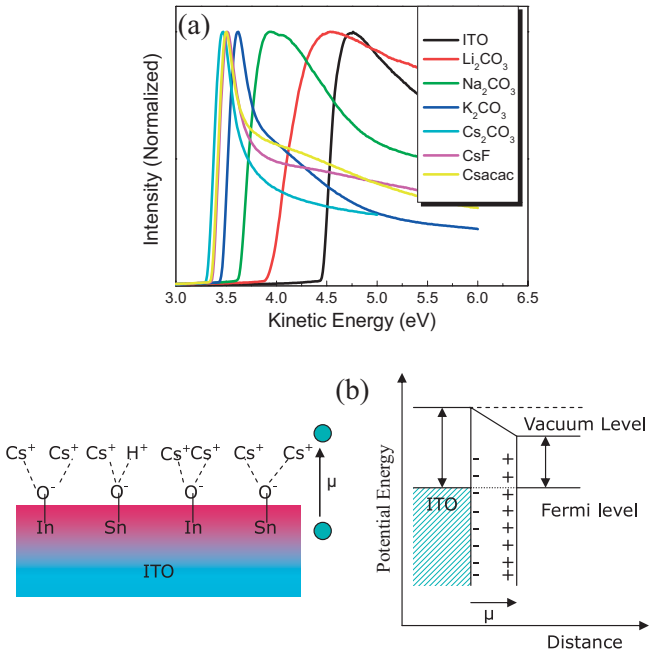

Figure 3. a) Evolution of secondary electron edge with different buffer layers on ITO, b) scheme for the formation of dipole layer on ITO and its effect on reducing the work function of ITO.

layer forms at the interface. The formation of such dipole layer can be explained by such scenario as illustrated in Figure 3b. A thin layer of O-M is formed at the ITO or FTO surface with metal ions in the vacuum side, where O and M stand for oxygen and metal species, respectively. The dipole points from ITO to vacuum and reduces the ITO surface work function. The dipole moment is directly related to the electron-donating ability of metal species. Since the change in ITO work function is proportional to dipole moment,[19] ITO surface with O-Cs dipole layer has the lowest effective work function owing to the highest dipole moment. The characteristics of inverted solar cell can be well correlated to this dipole layer: I_{SC} increases and series resistance reduces because of enhanced interfacial charge transfer rate at the cathode, and V_{OC}[20] increases because of lower cathode work function before Fermi energy pinning.[21] There are two possibilities for formation of O-M structure: i) positive metal ions are directly attracted by the negative oxygen ions from ITO itself, particularly after the UV ozone process; and ii) O-M replaces the hydroxyl group on the ITO surface by surface chemical reaction: –OH $+M^+ \rightarrow$ –O–Cs $+H^+$, similar to chemisorption of Cl-terminated molecules onto ITO.[18] In order to testify the possibility of chemisorption, the atom ratio of Cs and F was examined by XPS. CsF was chosen because it does not contain O or C species which might overlap signal from ITO substrate or ambient contamination. Another reason is that both Cs and F have high sensitivity in X-ray signal. The Cs/F ratio of 4.6–4.9 was obtained for CsF on ITO surface, which agrees with the second hypothesis (ii).

In summary, an important method is reported to take the full advantage of the solution fabrication process for the plastic electronic devices. A lamination process was invented by using the conductive polymer glue as the medium to form the device. This method has the advantage of being low cost, self-encapsulation, and providing high transparency for various applications. The preliminary results on solar cells show promising efficiency comparable to device by regular processing method, suggesting this method will open a new direction for future low-cost plastic electronic devices.

Experimental

For the device fabrication, the ITO substrates first underwent a routine cleaning procedure, which included sonication in detergent followed by repeated rinsing in deionized water, acetone, and isopropyl alcohol, and finally treatment with ultraviolet (UV) ozone. Poly(3,4-ethylenedioxythiophene): polystyrenesulfonate (PEDOT:PSS Baytron-P 4083) was first spin-cast onto an ITO/glass substrate at a spin speed of 4000 rpm, which corresponds to a thickness of 25 nm, and baked at 150 °C for 20 min before spin casting the polymer film. P3HT (purchased from Rieke Metals, used as received) was first dissolved in 1,2-dichlorobenzene (DCB) to make 17 mg mL^{-1} solution, followed by blending with PCBM (purchased from Nano-C, used as received) in 50 wt %. The blend was stirred for ca. 14 h at 40 °C in the glove box. The active layer was obtained by spin-coating the blend at 600 rpm. for 60 s and the thickness of film was ca. 210–230 nm, as measured with a Dektek profilometer. The active device area was 0.11 cm^2. Spin-coating at 600 rpm. left the films wet, which were then dried in covered glass petri dishes. Before cathode deposition, the films were thermally annealed at 110 °C for various times. Testing was done under simulated AM1.5G irradiation (100 mW cm^{-2}) using a xenon-lamp-based solar simulator (Oriel 96000 150W Solar Simulator)

Received: May 5, 2007
Revised: August 4, 2007
Published online: January 9, 2008

[1] M. Granstrom, K. Petritsch, A. C. Arias, A. Lux, M. R. Andersson, R. H. Friend, *Nature* **1998**, *395*, 257.
[2] N. S. Sariciftci, L. Smilowitz, A. J. Heeger, F. Wudl, *Science* **1992**, *258*, 1474.
[3] C. J. Brabec, J. A. Hauch, P. Schilinsky, C. Waldauf, *MRS Bull.* **2005**, *30*, 50.
[4] R. A. J. Janssen, J. C. Hummelen, N. S. Sariciftci, *MRS Bull.* **2005**, *33*, 50.
[5] C. W. Tang, *Appl. Phys. Lett.* **1986**, *48*, 183.
[6] P. Peumans, A. Yakimov, S. R. Forrest. *J. Appl. Phys.* **2003**, *93*, 3693.
[7] a) G. Li, V. Shrotriya, J. Huang, Y. Yao, T. Moriarty, K. Emery, Y. Yang, *Nat. Mater.* **2005**, *4* , 864. b) J. Huang, G. Li, Y. Yang, *Appl. Phys. Lett.* **2005**, *87*, 112105.
[8] V. Shrotriya, G. Li, Y. Yao, T. Moriarty, K. Emery, Y. Yang, *Adv. Funct. Mater.* **2006**, *16*, 2016.
[9] J. Huang, G. Li, E. Wu, Q. Xu, Y. Yang. *Adv. Mater.* **2006**, *18*, 114.
[10] J. Huang, T. Watanabe, K. Ueno, Y. Yang. *Adv. Mater.* **2007**, *19*, 739.
[11] J. Ouyang, Y. Yang. *Adv. Mater.* **2006**, *18*, 2141
[12] J. Huang, G. Li, Y. Yang, *Appl. Phys. Lett.* **2005**, *87*, 112105.
[13] V. Shrotriya, Y. Yao, G. Li, Y. Yang, *Appl. Phys. Lett.* **2006**, *89*, 063505.
[14] V. Shrotriya, E. Wu, G. Li, Y. Yao, Y. Yang, *Appl. Phys. Lett.* **2006**, *88*, 064104.

[15] J. Huang, P. F. Miller, J. S. Wilson, A. J. Mello, J. C. Mello, D. D. C. Bradley, *Adv. Funct. Mater.* **2005**, *15*, 290
[16] F. Yang, M. Shtein, S. R. Forrest. *Nat. Mater.* **2005**, *4*, 37.
[17] C. Waldauf, M. Morana, P. Denk, P. Schilinsky, K. Coakley, S. A. Choulis, C. J. Brabec, *Appl. Phys. Lett.* **2006**, *89*, 233517.
[18] J. Huang, Z. Xu, Y. Yang, *Adv. Funct. Mater.* **2007**, *17*, 1966
[19] S. Khodabakhsh, D. Poplavskyy, S. Heutz, J. Nelson, D. D. C. Bradley, H. Murata, T. S. Jones, *Adv. Funct. Mater.* **2004**, *14*, 1205.
[20] S. Khodabakhsh, B. M. Sanderson, J. Nelson, T. S. Jones. *Adv. Funct. Mater.* **2006**, *16*, 95.
[21] C. J. Brabec, A. Cravino, D. Meissner, N. S. Sariciftci, T. Fromherz, M. T. Rispens, L. Sanchez, J. C. Hummelen, *Adv. Funct. Mater.* **2001**, *11*, 374.

